iScience

CellPress
OPEN ACCESS

Article

Inhibition of CD44 suppresses the formation of fibrotic scar after spinal cord injury via the JAK2/STAT3 signaling pathway

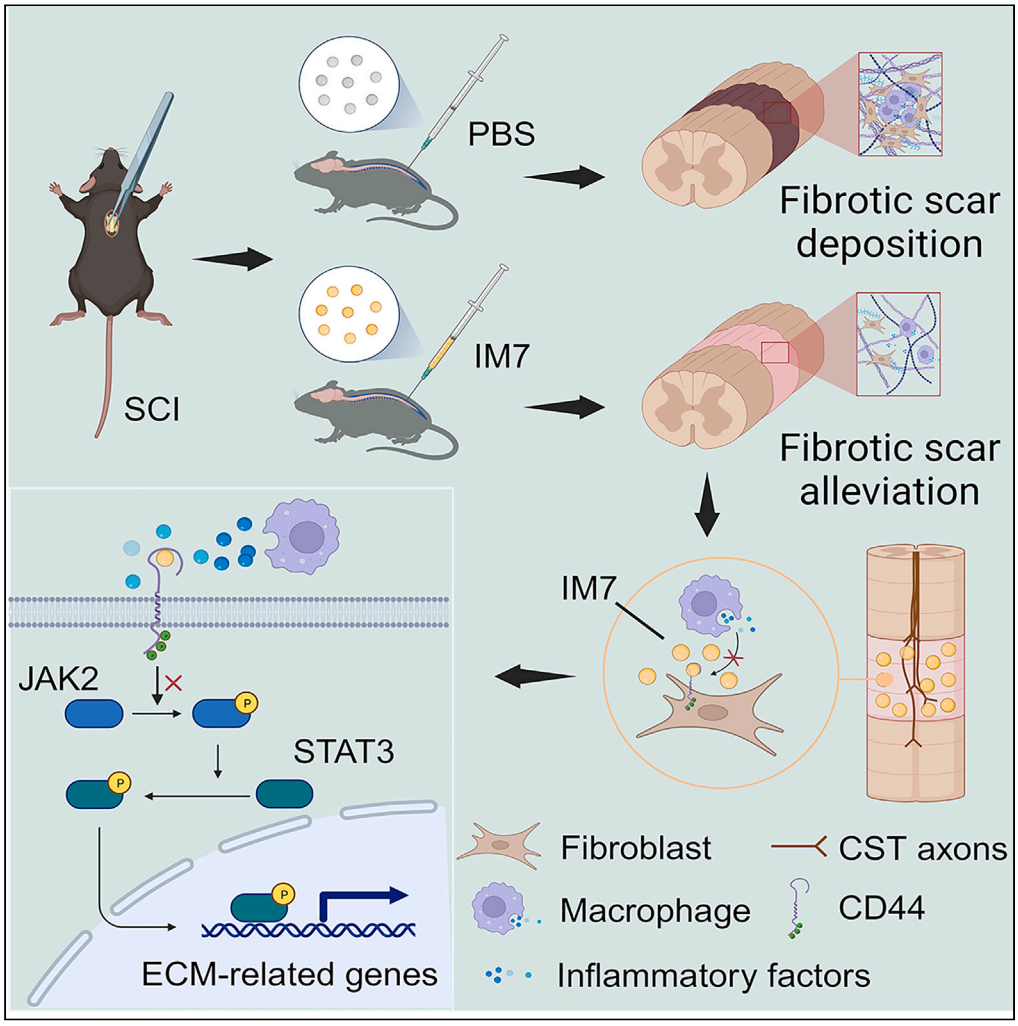

Jin Guo, Tuo Yang, Weizhong Zhang, ..., Xiaosong Gu, Rangjuan Cao, Shusen Cui

nervegu@ntu.edu.cn (X.G.)
caorj@jlu.edu.cn (R.C.)
cuiss@jlu.edu.cn (S.C.)

Highlights

CD44 blockade alleviates fibrotic scar formation after spinal cord injury

Inhibition of CD44 facilitates functional recovery following spinal cord injury

CD44 promotes ECM expression in fibroblasts in the inflammatory microenvironment

CD44 regulates ECM expression via the JAK2/STAT3 pathway in fibroblasts

Guo et al., iScience 27, 108935
February 16, 2024
https://doi.org/10.1016/j.isci.2024.108935

iScience

CellPress
OPEN ACCESS

Article

Inhibition of CD44 suppresses the formation of fibrotic scar after spinal cord injury via the JAK2/STAT3 signaling pathway

Jin Guo,[1,2] Tuo Yang,[1,2] Weizhong Zhang,[1,2] Kaiming Yu,[1,2] Xiong Xu,[1,2] Weizhen Li,[1,2] Lili Song,[3] Xiaosong Gu,[4,*] Rangjuan Cao,[1,2,5,*] and Shusen Cui[1,2,*]

SUMMARY

Fibrotic scar is one of the main impediments to axon regeneration following spinal cord injury (SCI). In this study, we found that CD44 was upregulated during the formation of fibrotic scar, and blocking CD44 by IM7 caused downregulation of fibrosis-related extracellular matrix proteins at both 2 and 12 weeks post-spinal cord injury. More Biotinylated dextran amine (BDA)-traced corticospinal tract axons crossed the scar area and extended into the distal region after IM7 administration. A recovery of motor and sensory function was observed based on Basso Mouse Scale (BMS) scores and tail-flick test. *In vitro* experiments revealed that inhibiting CD44 and JAK2/STAT3 signaling pathway decreased the proliferation, differentiation, and migration of fibroblasts induced by the inflammatory supernatant. Collectively, these findings highlight the critical role of CD44 and its downstream JAK2/STAT3 signaling pathway in fibrotic scar formation, suggesting a potential therapeutic target for SCI.

INTRODUCTION

Traumatic spinal cord injury (SCI) is a common injury to the central nervous system (CNS). Globally, approximately 180,000 SCI patients with permanent paralysis are recorded each year.[1] In addition to the limited regenerative capacity of the mature CNS, another crucial factor affecting functional recovery is the formation of fibrotic scar, which hinders precursor cells from entering the injured site and promoting axon regeneration.[2] Furthermore, this structure can release inhibitory molecules, such as tenascin-C, ephrinB2, and NG2,[3] ultimately leading to poor recovery of extremity function. Therefore, reducing fibrotic scar formation after SCI is a major clinical challenge.

It has been reported that CNS fibroblasts play a significant role in fibrotic scar formation.[4] These fibroblasts are primarily located in the perivascular space, meninges, and peripheral choroid plexus.[5,6] Following SCI, the fibroblasts proliferate, migrate, and accumulate in the core area from the third day, increasing remarkably on the fifth day, and reaching their peak on the seventh day.[3] During this time, large amounts of extracellular matrix (ECM) proteins, mainly collagen, fibronectin, and laminin, are secreted by fibroblasts and deposited to form a fibrotic network structure on the 14th day, which finally results in the formation of dense fibrotic scar tissue.[3,7] Meanwhile, a large number of reactive astrocytes proliferate with Chondroitin sulfate proteoglycans (CSPGs) secreting, which ultimately forms astrocyte scar and tightly wraps around the fibrotic scar area[8,9] (Figure 1A). The inflammatory microenvironment following SCI also plays a significant role in this process.[10] By 3 dpi (days post injury), monocytes differentiate into macrophages that phagocytose cellular debris and tissue fragments, secrete various cytokines and inflammatory factors, and recruit fibroblasts to participate in the subsequent repair process, collectively creating a local inflammatory microenvironment during the early stage of injury.[8,11,12] Therefore, targeting fibroblasts under the inflammatory microenvironment after SCI may be an effective strategy to reduce fibrotic scar and improve functional recovery.

The TGF-β1/Smad pathway is the classical and widely accepted mechanism implicated in promoting fibrotic scar formation after SCI.[13] However, given its involvement in diverse physiological and pathological processes, systemic application of TGF-β1 inhibitor may lead to systemic sclerosis and other diseases.[14] Therefore, it is imperative to explore safer and more effective strategies to resolve fibrosis. Numerous studies have reported that CD44, a type-I transmembrane glycoprotein, participates in inflammation and tissue fibrosis.[15–18] CD44 is widely expressed in most vertebrate cells, including fibroblasts.[19–21] As a cell adhesion molecule, CD44 plays a role in cell-cell and cell-matrix

[1]Department of Hand and Foot Surgery, China-Japan Union Hospital of Jilin University, Changchun, Jilin Province 130033, China
[2]Key Laboratory of Peripheral Nerve Injury and Regeneration of Jilin Province, Changchun, Jilin Province 130033, China
[3]Department of Hand & Microsurgery, Peking University Shenzhen Hospital, Shenzhen 518036, China
[4]Key Laboratory of Neuroregeneration of Jiangsu and Ministry of Education, Co-innovation Center of Neuroregeneration, Nantong University, Nantong, Jiangsu 226001, China
[5]Lead contact
*Correspondence: nervegu@ntu.edu.cn (X.G.), caorj@jlu.edu.cn (R.C.), cuiss@jlu.edu.cn (S.C.)
https://doi.org/10.1016/j.isci.2024.108935

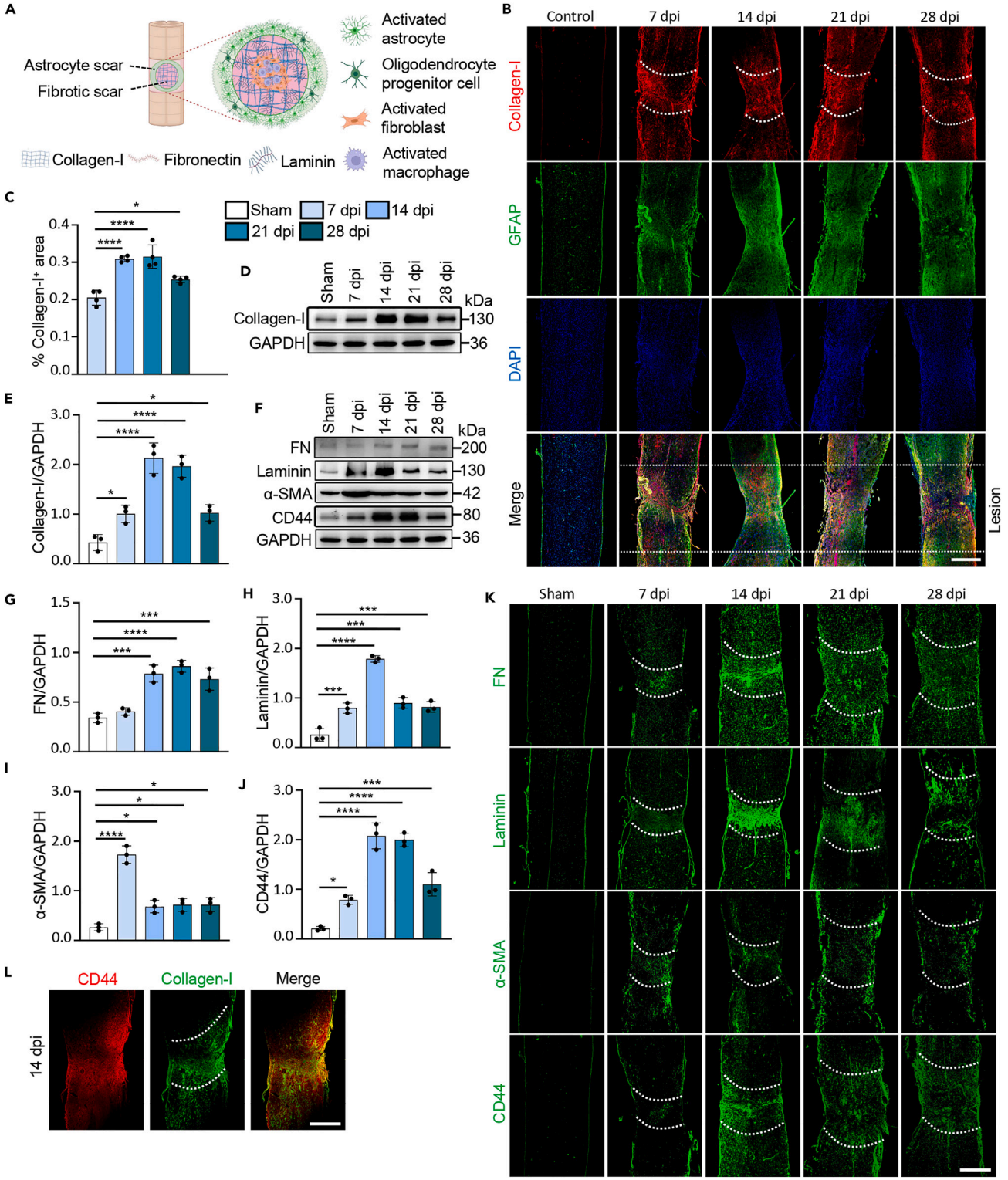

Figure 1. The expression of CD44 and fibrosis-related proteins were upregulated after SCI

(A) Diagram of fibrotic scar composition of spinal cord after SCI.

(B) Control and injured spinal cord sections collected at different times (7 dpi, 14 dpi, 21 dpi, and 28 dpi) after SCI were stained for collagen-I (red), GFAP (green) and cell nucleus (DAPI). The white dotted lines showed the areas of fibrotic scar and lesion regions at different groups. Scale bar, 400 μm.

Figure 1. *Continued*

(C) Quantification of collagen-I^{+} area in B (n = 4) by one-way ANOVA.

(D) Western blotting determined the expression of collagen-I at different times after SCI.

(E) Quantitative expression of collagen-I in D (n = 3) by one-way ANOVA.

(F) Western blotting determined the expression of fibronectin (FN), laminin, α-SMA, and CD44 at different times after SCI.

(G–J) Quantification of western blotting results in F. N = 3 of each group by one-way ANOVA.

(K) Representative immunofluorescent staining images of fibronectin (FN), laminin, α-SMA, and CD44 at different times after SCI. The white dotted lines showed the areas of scar region at different groups. Scale bar, 400 μm.

(L) Representative immunofluorescent staining images for CD44 (red) and collagen-I (green) at 14 dpi. Scale bar, 400 μm. All data were presented as mean ± SEM (*p < 0.05, ***p < 0.001, ****p < 0.0001). (See also Figure S1).

interactions[22] in various pathological processes, such as lymphocyte infiltration,[23,24] wound healing, and scar formation.[17] In a myocardial fibrosis remodeling model, CD44 promoted ECM deposition and cardiac remodeling.[18] However, whether CD44 is involved in the formation of fibrotic scar after SCI and its underlying mechanisms remain unknown.

In this study, we found that the expression of CD44, consistent with the fibrosis-related ECM proteins, was significantly upregulated after SCI. CD44 blocking reduced the formation of fibrotic scar in both the acute and chronic stages of SCI, and ultimately promoted the functional recovery of the spinal cord. *In vitro*, inflammatory supernatant (IS) induced CD44 expression, mediating fibroblast migration, proliferation, and the secretion of fibrosis-related proteins. Mechanistic studies have revealed that CD44 modulates fibrotic scar formation under the inflammation microenvironment via the JAK2/STAT3 signaling pathway. This finding highlights CD44 as a potential new therapeutic target for the treatment of fibrotic scar following SCI.

RESULTS

The expression of CD44 and fibrosis-related proteins were upregulated after SCI

To characterize the expression of proteins associated with fibrotic scar after SCI, control or injured spinal cord tissues collected at 7 dpi, 14 dpi, 21 dpi, and 28 dpi were proceeded to immunofluorescent staining. Glial fibrillary acidic protein (GFAP), a marker of reactive astrocytes used to identify astrocyte scar, was co-stained with collagen-I, which was the vital component of fibrotic scar enclosed by astrocyte scar. Results showed that the lesion areas did not change significantly in a month after SCI (Figures 1B and S1A). Compared to control group, collagen-I began to increase at 7 dpi, reaching the peak at 14 dpi and 21 dpi in the core area, and maintained the high expression at 28 dpi (Figures 1B and 1C). The expression tendency of collagen-I was further confirmed by western blotting (Figures 1D and 1E). After that, other fibrosis-related ECMs, fibronectin, laminin, and α-SMA, were also assessed. The expression pattern of fibronectin and laminin were consistent with that of collagen-I. However, α-SMA, a marker of fibroblast differentiation into myofibroblast, showed a slightly different pattern with the highest expression at 7 dpi (Figures 1F–1I, 1K and S1B–S1D). These findings were consistent with earlier reports,[3] suggesting that fibrotic scar formation primarily occurs two weeks after SCI. Intriguingly, CD44 was upregulated as early as 7 dpi and maintained high expression at 14 dpi and 21 dpi, consistent with the tendency of fibrosis-related proteins (Figures 1F, 1J, 1K, and S1E). Additionally, CD44 was closely correlated to collagen-I after SCI (Figure 1L), suggesting its involvement in the formation of fibrotic scar after SCI.

Next, we examined the relationship between CD44 and GFAP by immunofluorescent staining at 14 dpi after SCI, when both of them showed high expression. Intriguingly, CD44 was not co-localized with GFAP-positive astrocytes (Figure S1F). Therefore, we investigated whether CD44 was derived from fibroblasts by staining with Thy-1, a marker of fibroblast. Results showed that CD44 mainly located on Thy-1 positive cells. Additionally, we also examined the expression of CD44 on BJ-1 fibroblasts by immunocytochemical staining, which showed widespread CD44 on the surface of the cells (Figures S1G and S1H). Together, these results suggest that CD44 primarily influences the development of fibrotic scar via fibroblasts rather than astrocyte scar.

Inhibition of CD44 downregulated the expression of fibrosis-related proteins in 2 weeks post spinal cord injury

To investigate the involvement of CD44 in the formation of fibrotic scar after SCI, we employed the IM7 monoclonal antibody, which specifically binds to extracellular domain of CD44 and blocks its function *in vivo* and *in vitro*. Given the tendency for fibroblast proliferation and the increased expression of fibrosis-related proteins after SCI, intrathecal injections of either 10 μg or 20 μg IM7 in 20 μL of PBS were administered starting from the 5th day after surgery, with injections given every other day. A control group received an equivalent volume of sterile PBS (Figures 2A and 2B). Immunostaining was conducted to examine the expression of collagen-I and GFAP in different groups (Figure 2C). Results showed that the lesion areas of these three groups were not affected (Figures 2C and S2A), the expression and distribution density of collagen-I at the injury site were significantly reduced after the administration of IM7 at both doses treatments, consistent with the results by western blotting (Figures 2C–2F). In addition, similar reductions were observed in the expression of fibronectin, laminin, and α-SMA (Figures 2G–2K and S2B–S2D). These results suggested that CD44 inhibition impaired the expression of fibrosis-associated proteins. Interestingly, Quantitative analysis showed that GFAP did not change significantly after low dose IM7 treatment (10 μg), but was reduced when injected at a higher dose (20 μg) (Figures 2C and S2E–S2G), and was still predominantly localized around CD44 in the injury core area (Figure S2H). This finding suggested that a high dose of IM7 may affect GFAP and/or astrocyte scar formation. Therefore, a dose of 10 μg IM7 administration appeared to be effective in downregulating the expression of fibrosis-related proteins without altering astrocyte scar in 2 weeks.

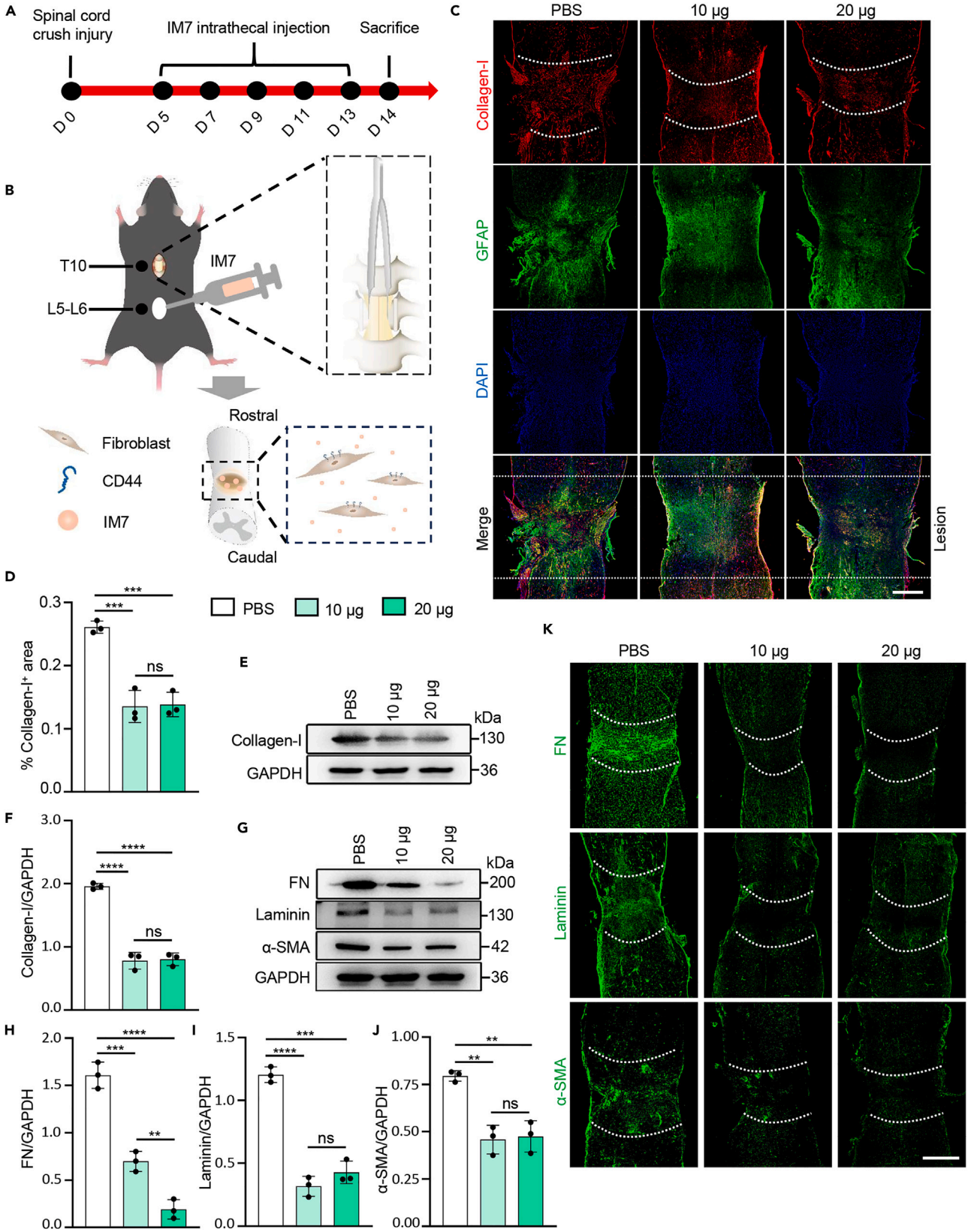
A
Spinal cord crush injury
IM7 intrathecal injection
Sacrifice
D0
D5
D7
D9
D11
D13
D14
B
T10
L5-L6
IM7
Rostral
Caudal
Fibroblast
CD44
IM7
C
PBS
10 μg
20 μg
Collagen-I
GFAP
DAPI
Merge
Lesion
D
PBS
10 μg
20 μg
% Collagen-I+ area
ns
E
PBS
10 μg
20 μg
kDa
Collagen-I
GAPDH
130
36
F
Collagen-I/GAPDH
ns
G
PBS
10 μg
20 μg
kDa
FN
Laminin
α-SMA
GAPDH
200
130
42
36
H
FN/GAPDH
I
Laminin/GAPDH
ns
J
α-SMA/GAPDH
ns
K
PBS
10 μg
20 μg
FN
Laminin
α-SMA

Figure 2. Inhibition of CD44 downregulated the expression of fibrosis-related proteins in 2 weeks post spinal cord injury

(A) Flow chart of 2-week experiment *in vivo* after SCI.

(B) Diagram of mouse spinal cord crush injury and IM7 intrathecal injection.

(C) Spinal cord sections were stained for collagen-I (red), GFAP (green), and cell nucleus (DAPI). The white dotted lines showed the areas of fibrotic scar and lesion regions at different groups. Scale bar, 400 μm.

(D) Quantification of collagen-I^{+} area in C (n = 3) by one-way ANOVA.

(E) Western blotting determined the expression of collagen-I at different groups after SCI.

(F) Quantitative expression of collagen-I in E (n = 3) by one-way ANOVA.

(G) Western blotting determined the expression of FN, laminin, and α-SMA at different groups after SCI.

(H–J) Quantification of western blotting results in G. N = 3 per group by one-way ANOVA.

(K) Spinal cord sections were stained for FN, laminin, and α-SMA at different groups after SCI. The white dotted lines showed the areas of scar region at different groups. Scale bar, 400 μm. All data were presented as mean ± SEM (**p < 0.01, ***p < 0.001, ****p < 0.0001). (See also Figure S2).

Blockage of CD44 alleviated the chronic fibrotic scar formation and promoted functional recovery of the spinal cord

To investigate the effects of CD44 inhibition on the chronic fibrotic scar after SCI, we administered 10 μg of IM7 as previously described. Behavioral tests, Basso Mouse Scale (BMS) scores and the tail-flick test, were performed after the final injection and continued weekly until the 12th week, when spinal cord tissues were collected (Figure 3A). Immunohistochemistry staining revealed that the spinal cord tissue in the control group exhibited interruption, with an abundance of collagen-I in the core area of the injury site. In contrast, significant reductions in lesion areas were observed in the IM7 group (Figures 3B and S2I). Meanwhile the expression of collagen-I reduced remarkably (Figures 3B and 3C), consistent with the results of western blotting (Figures 3D and 3E). Moreover, the area of fibrotic scar decreased significantly (Figure 3F), suggesting that CD44 blockade could inhibit collagen-I and fibrotic scar formation even a long time after injury. Additionally, the expression levels of fibronectin, laminin, and α-SMA were downregulated in the IM7 group, and exhibited dispersed distribution (Figures 3G–3K and S2J–S2L). As expected, the upregulation of GFAP expression was not influenced by IM7 treatment (Figures S2M and S2N). These results indicated that CD44 interruption at the early stage of injury had a significant inhibitory effect on chronic fibrotic scar formation.

Next, we administered a Biotinylated dextran amine (BDA) injection to explore whether IM7 could facilitate the crossing of regenerated axons through the fibrotic scar. BDA was injected into the left cerebral cortex at the 10th week, and the spinal cord was collected 2 weeks later for immunohistochemistry staining. In the control group, the labeled corticospinal tract (CST) axons primarily migrated and aggregated on the rostral side, but few of them crossed the fibrotic scar area. However, in the IM7 group, more labeled CST axons were observed at both ends of the injury area, indicating an axon regeneration through the scar (Figure 4A). Moreover, we conducted a BDA injection three days before SCI, and then the spinal cord was collected two weeks later to explore whether there were any spared CST axons in the distal region of the injury site in the early stage of SCI. Results showed that there were no BDA-labeled CST axons in the distal region, suggesting that no spared axons existed after SCI (Figure 4A).

We calculated the BMS scores and conducted the tail-flick test after IM7 treatment to evaluate for functional recovery. In the sham group, BMS scores remained largely unaffected after surgery. However, the scores dropped to 0 by the 2nd week postoperatively in the control and IM7 groups simultaneously. Subsequently, BMS scores gradually increased from the 4th week in both groups, whereas a more pronounced increase was observed in IM7 group. By the 12th week, mice receiving IM7 generally displayed frequent rearfoot stirrups and occasional stable footsteps, indicating some recovery of spinal cord motor function. However, a complete restoration was not achieved, and the BMS scores barely reached 4. In contrast, mice in the control group exhibited ankle joint movements but rarely rearfoot stirrups, resulting in BMS scores averaging around 2 (Figure 4B). The tail-flick test revealed that in the sham group, the mean tail-flick time remained consistently around 0.90 s. However, in the control and IM7 groups, the time increased to 2.33 s and 2.69 s, respectively, in the 2nd week postoperatively. Notably, the latency in the IM7 group was marginally longer compared to the control group at this point. This may be attributed to the transient stress response triggered by the IM7 injection. Moreover, there was a significant reduction in tail-flick latency in the IM7 group from the 3rd week through the 8th week. Interestingly, the latency in the IM7 group was comparable to that in the sham group at 7th week, while in the control group until to the 9th week. From the 9th week onward, no notable differences were observed among these three groups, suggesting that sensory function recovery after SCI was more evident and potentially superior to motor function recovery, and the sensory recovery of IM7 group was better than that in the control group (Figure 4C). Together, these behavioral results indicated that CD44 blockade promoted the functional recovery of the spinal cord.

CD44 promoted fibroblasts function in the inflammatory microenvironment *in vitro*

To investigate the role of CD44 in the inflammatory microenvironment, IS was collected 24 h after the administration of Lipopolysaccharide (LPS) to macrophages and then administered to BJ-1 fibroblasts for various durations (6 h, 24 h, 48 h, and 72 h) (Figure S2O). Western blotting revealed an upregulation of CD44 upon stimulation with IS, with a notable increase observed at 24 h (Figures 5A and 5B). Similarly, the expression of α-SMA and collagen-I gradually increased and also reached their peak at 24 h (Figures 5A, 5C, and 5D). These findings indicated that the IS promoted functional changes in fibroblasts *in vitro*.

Next, IM7 was used to block CD44 in BJ-1 fibroblasts in the inflammatory microenvironment. Western blotting results demonstrated that the increased expression of α-SMA induced by IS was interrupted after the addition of IM7. Intriguingly, even in the presence of a control supernatant (CS), IM7 was also able to inhibit the expression of α-SMA, indicating that endogenous CD44 has an effect on fibroblast

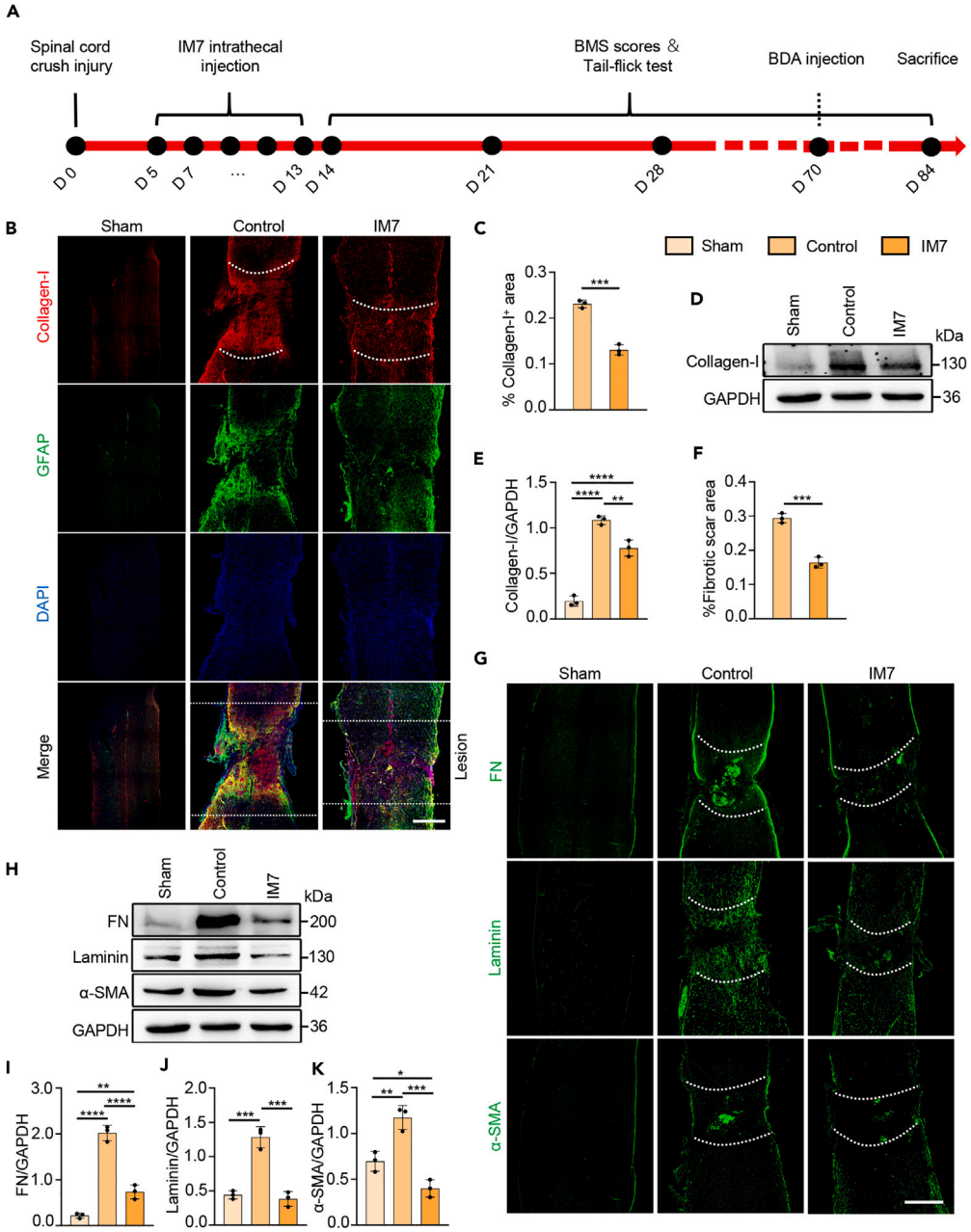

Figure 3. Inhibition of CD44 suppressed the formation of chronic fibrotic scar

(A) Flow chart of 12-week experiment *in vivo* after SCI.

(B) Spinal cord sections were stained for collagen-I (red), GFAP (green), and cell nucleus (DAPI). The white dotted lines showed the areas of fibrotic scar and lesion regions at different groups. Scale bar, 400 μm.

(C) Quantification of collagen-I^{+} area in B (n = 3) by unpaired Student's t-tests.

(D) Western blotting determined the expression of collagen-I at different groups.

(E) Quantitative expression of collagen-I in D. N = 3 per group by one-way ANOVA.

(F) Quantification of fibrotic scar area in B (n = 3) by unpaired Student's t-tests.

(G) Spinal cord sections were stained for FN, laminin and α-SMA at different groups. The white dotted lines showed the areas of scar region at different groups. Scale bar, 400 μm.

(H) Western blotting determined the expression of FN, laminin, and α-SMA at different groups.

(I–K) Quantification of western blotting results in H. N = 3 of each group by one-way ANOVA. All data were presented as mean ± SEM (*p < 0.05, **p < 0.01, ***p < 0.001, ****p < 0.0001). (See also Figure S2).

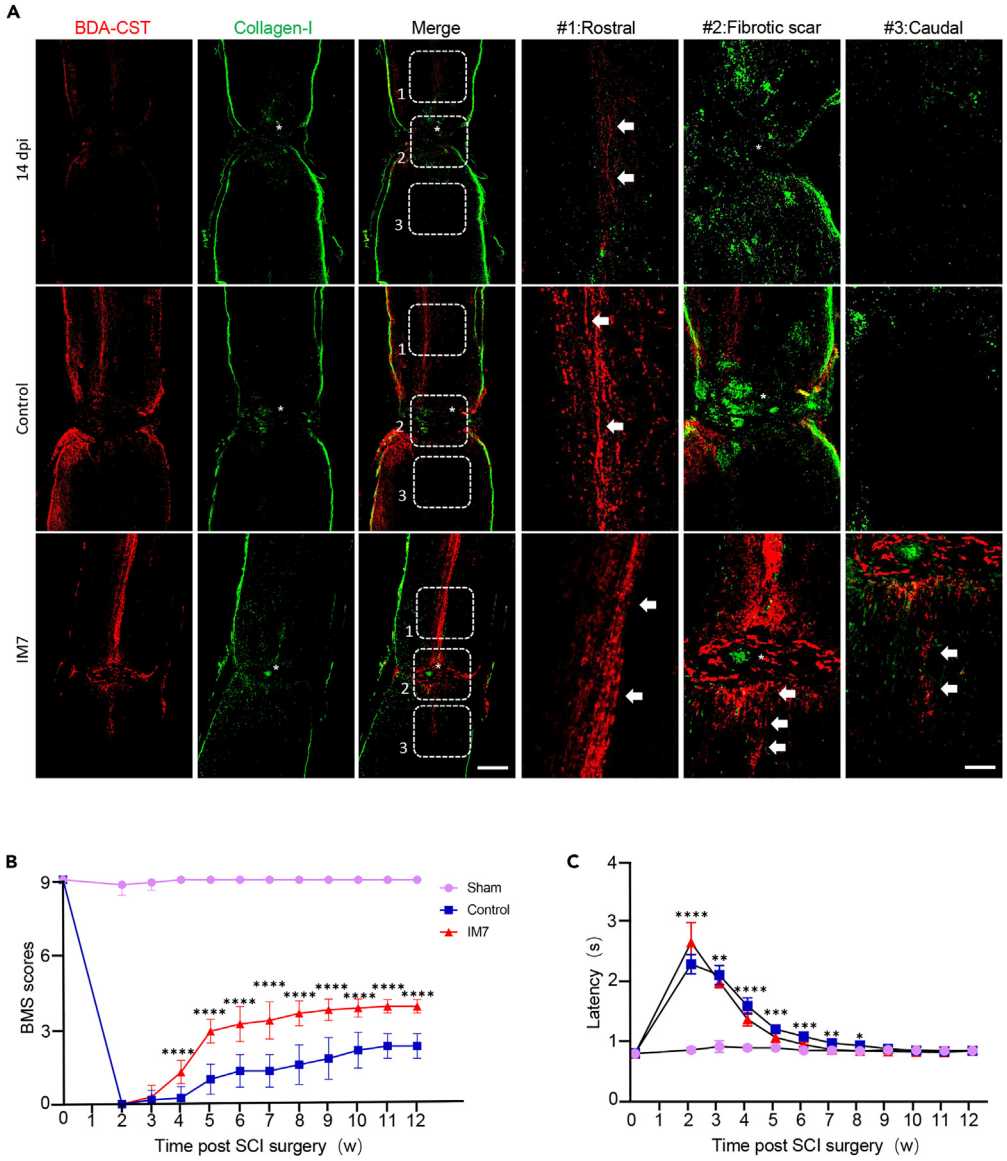

Figure 4. Inhibition of CD44 promoted the crossing of CST axons through the fibrotic scar region and improved functional recovery of spinal cord

(A) Representative images of BDA-labeled CST axons (red) and collagen-I (green) at early injury stage (14 dpi) after SCI and different treatment groups after 12 weeks (control and IM7 group). Scale bar, 500 μm or 100 μm. The white arrows indicated the process of CST axons. The asterisk showed the region of fibrotic scar.

(B and C) Quantification analysis for BMS scores (B) in terms of motor function and tail-flick test (C) for sensory function. All data were presented as mean ± SEM (*p < 0.05, **p < 0.01, ***p < 0.001, ****p < 0.0001). The asterisk signs indicated the difference between the control and IM7 group (n = 10 for sham group, n = 12 for control group and n = 14 for IM7 group by two-way ANOVA).

differentiation (Figures 5E and 5F). Besides, the upregulation of collagen-I, fibronectin, and laminin induced by the IS stimulation was restored to levels in the control group following CD44 inhibition (Figures 5E and 5G–5I).

We also analyzed cell migration and proliferation of fibroblasts in the inflammatory microenvironment (Figures 5J and 5K). Transwell assay revealed that, regardless of CD44 inhibition or not, only a small number (19 versus 17 per 10^6 μm^2) of fibroblasts migrated under CS. In contrast, the mean number increased to 65 per 10^6 μm^2 when stimulated by IS, but dropped to 23 upon CD44 inhibition (Figures 5J and 5L). To investigate fibroblast proliferation, the EdU kit was applied following control or IS treatment. In the control group, the proliferation was not affected by IM7, with a mean proliferation rate per 10^6 μm^2 of 10.7% or 8.4%, respectively. However, when fibroblasts were stimulated with IS, a significantly higher proliferation rate of 30.6% was observed. Notably, when CD44 was pre-inhibited, the proliferation rate decreased again to 11.7% (Figures 5K and 5M). Taken together, these results suggest that CD44 plays a crucial role in fibroblast differentiation, migration, and proliferation in the inflammatory microenvironment.

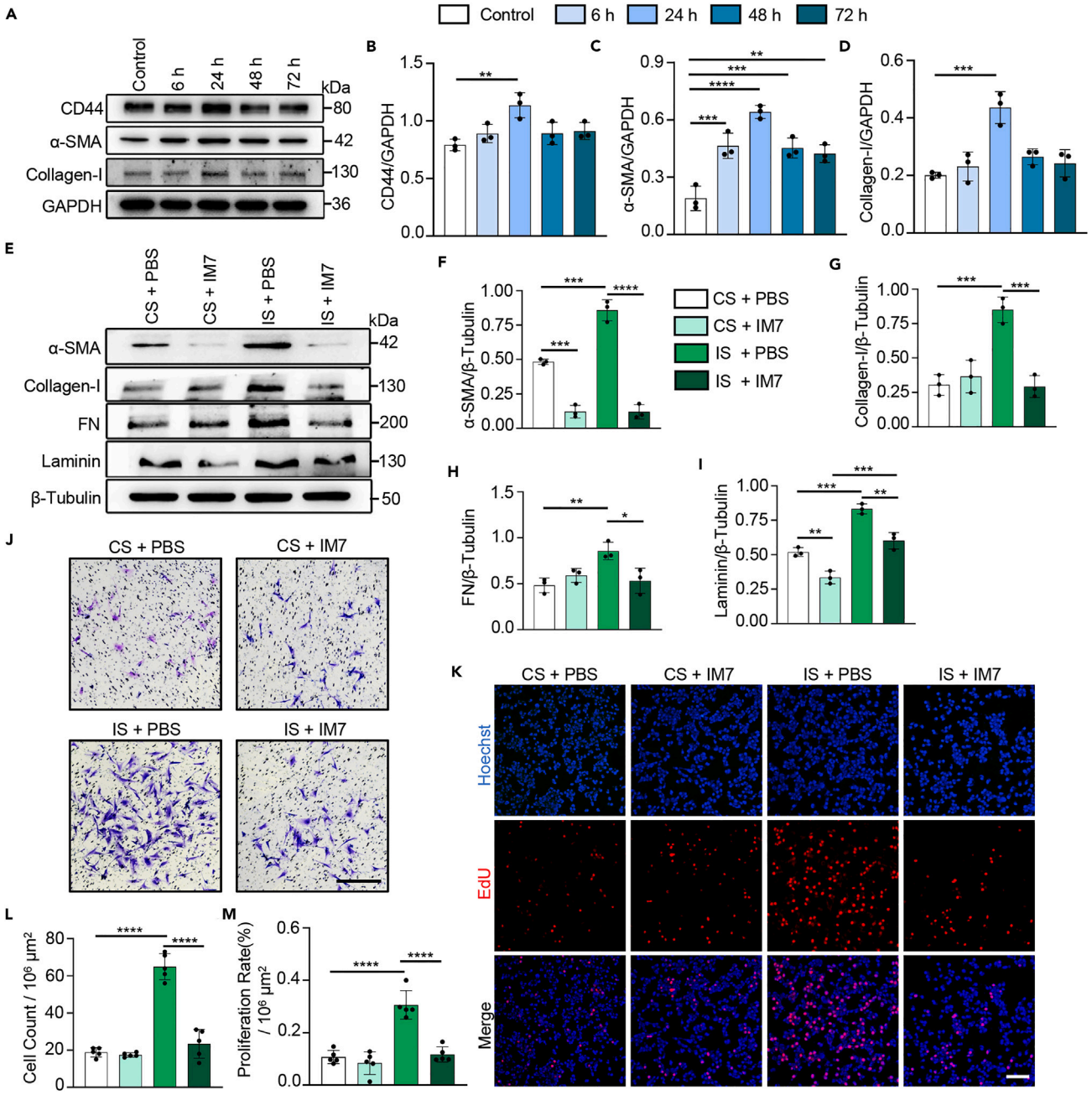

Figure 5. CD44 was a key molecule in the inflammatory microenvironment that promoted fibroblasts proliferation, differentiation and migration

(A) Western blotting analyzed the expression of CD44, α-SMA, and collagen-I at different time points (6 h, 24 h, 48 h, and 72 h) in BJ-1 fibroblasts *in vitro* after stimulation with inflammatory supernatant (IS).

(B–D) Quantification of western blotting results in A. N = 3 of each group by one-way ANOVA.

(E) Western blotting analyzed the expression of α-SMA, collagen-I, FN and laminin in the BJ-1 fibroblasts *in vitro* subjected to IS stimulation after inhibition of CD44.

(F–I) Quantification of Western blotting results in E. N = 3 of each group by one-way ANOVA.

(J) Representative images of cell transwell assay in different groups. Scale bar, 400 μm.

(K) Representative images of cell EdU assay in different groups. Scale bar, 200 μm.

(L and M) Quantification analysis of the cell numbers of migration (L) per 10^6 μm^2 (n = 5) and the rates of proliferation (%) (M) per 10^6 μm^2 (n = 5) in different groups. All data were presented as mean ± SEM. (*p < 0.05, **p < 0.01, ***p < 0.001, ****p < 0.0001). (See also Figure S2).

Involvement of the JAK2/STAT3 signaling pathway in CD44-mediated fibrotic effects in the inflammatory microenvironment

To determine the possible molecular mechanisms of CD44-mediated fibrosis, we initially explored the relationship between CD44 and the Smad family, which is well-known for its involvement in tissue fibrosis.[13] However, western blotting analysis showed that inhibition of CD44 with IM7 did not alter the expression of *p*-Smad2 in the inflammatory microenvironment (Figures 6A and 6B), suggesting that *p*-Smad2 did not mediate the effect of CD44. Previous studies have demonstrated that TGF-β1 signaling can induce STAT3-dependent fibrotic response by activation of JAK2, and activated STAT3 can participate in CD44-induced tissue fibrosis.[25–27] Therefore, we quantified the levels of *p*-JAK2/JAK2, p-STAT3/STAT3 in fibroblasts in the presence of the IS alone or in combination with IM7. Western blotting analysis revealed that *p*-JAK2 and p-STAT3 were significantly upregulated by inflammatory stimulation, but reduced after the inhibition of CD44 by IM7. Accordingly, the expression of JAK2 and STAT3 were decreased when *p*-JAK2 and p-STAT3 were elevated (Figures 6A–6F). These results suggest that IM7 administration blocked the activation of JAK2/STAT3 signaling pathway in the inflammatory microenvironment.

To clarify whether JAK2/STAT3 signaling molecules participated in CD44-mediated fibrosis, we used WP1066, a JAK2/STAT3 signaling pathway inhibitor, to inhibit both JAK2 and STAT3. Results showed that the enhanced expression of *p*-JAK2 and p-STAT3 induced by IS was suppressed after WP1066 treatment (Figures 6G–6I), while *p*-Smad2 remained unaffected (Figures 6G and 6J), indicating that JAK2/STAT3 might act independently of the Smad signaling pathway. Consistently, the increased levels of α-SMA, collagen-I, fibronectin, and laminin were all reduced following inhibition of the JAK2/STAT3 pathway (Figures 6K–6O). Notably, inhibiting the JAK2/STAT3 pathway did not decrease the expression of CD44 induced by IS (Figures 6K and 6P), suggesting that CD44 may be an upstream regulator of the JAK2/STAT3 signaling pathway.

We also examined the proliferation and migration of fibroblasts when JAK2/STAT3 was inhibited. EdU assay results showed that the mean proliferation rate per 10^6 μm^2 of fibroblasts decreased from 14.1% to 10.1% upon IS stimulation and from 5.9% to 3.1% upon CS stimulation, indicating that JAK2/STAT3 participated in fibroblast proliferation in both physiological and inflammatory conditions. However, in both groups treated with WP1066, the proliferation ability of cells in IS (10.1%) was stronger than that in control group (3.1%) (Figures 6Q and S3A), suggesting that other molecular mechanisms may be involved in this process. The cell migration assay showed that the mean number of migrated cells per 10^6 μm^2 decreased from 45 to 34 upon inhibition of the JAK2/STAT3 signaling pathway under IS stimulation (Figures 6R and S3B). Taken together, these results suggest that the JAK2/STAT3 signaling pathway may act as downstream molecules of CD44, contributing to the functional promotion of fibroblasts in the inflammatory microenvironment.

STAT3 as the downstream of JAK2 in CD44-mediated fibrotic effects in the inflammatory microenvironment

Since WP1066 can simultaneously block both JAK2 and STAT3, we employed AG490, a specific JAK2 inhibitor, to gain deeper insights into the downstream pathway of CD44. Western blotting analysis revealed that the elevated levels of *p*-JAK2 induced by IS were effectively reduced by AG490, as anticipated. However, it was noteworthy that the administration of AG490 also led to a decrease expression of STAT3 and p-STAT3, indicating that STAT3 functions downstream of JAK2 (Figures 7A–7D). Correspondingly, the levels of *p*-Smad2 and CD44 expression remained unaltered under these conditions (Figures 7A and 7E–7G), suggesting JAK2 likely serves as the key molecule between CD44 and STAT3, with minimal involvement in the Smad signaling pathway. Furthermore, the inhibition of JAK2 following IS treatment resulted in reduced expression of α-SMA, collagen-I, fibronectin, and laminin (Figures 7F and 7H–7K).

Notably, the EdU assay demonstrated a similar decrease in fibroblast proliferation when JAK2 was inhibited in the inflammatory microenvironment. However, no difference in proliferation was observed when a CS was used (Figures 7L and S3C). The transwell assay further confirmed the abolishment of migratory potential induced by IS after AG490 administration (Figures 7M and S3D). Collectively, these results strongly indicate that inhibition of JAK2 affected p-STAT3 and blocked the effect of CD44 on the proliferation and migration of fibroblasts in the inflammatory microenvironment. This suggests that STAT3 acts downstream of JAK2 in the CD44-mediated fibrotic effect within the inflammatory microenvironment.

DISCUSSION

In this study, we investigated the role of CD44 in fibroblast-mediated fibrotic scar formation following SCI and explored the underlying molecular mechanisms. Results indicated that CD44 expression was progressively increased after SCI, and this was accompanied by expression of fibrosis-related proteins. Inhibition of CD44 caused a reduction in the expression of these proteins and decreased fibrotic scar formation at both 2 weeks and 12 weeks after SCI. Moreover, more BDA-labeled CST axons traversed the fibrotic scar, and functional recovery, as indicated by BMS scores and the tail-flick test, was partially restored. Mechanistic experiments revealed that the upregulated expression of *p*-JAK2 and p-STAT3 in the inflammation supernatant was blocked when CD44 was inhibited. Suppression of the JAK2/STAT3 pathway led to the abolishment of CD44-mediated expression of fibrosis-related proteins, as well as the proliferation and migration of fibroblasts.

Spinal cord scar tissue after SCI is commonly classified into two types: astrocyte scar and fibrotic scar.[3] The former is mainly composed of reactive astrocytes and large amounts of CSPGs.[28] Researchers hold the view that astrocyte scar and inhibitory CSPGs can prevent axonal regeneration.[29] However, this conclusion remains controversial as studies have reported potential benefits of astrocyte scar for axon regeneration, as spontaneous axon regeneration did not occur when astrocytes were immediately removed after SCI.[30]

Consequently, more studies have shifted their focus toward the fibrotic scar and its crucial inhibitory effect on spinal cord function following SCI.[31–34] The fibrotic scar primarily comprises fibroblasts, myofibroblasts, and an excessive amount of ECM proteins, with fibroblasts being the key components of this specialized structure.[11,35] Under normal physiological conditions, fibroblasts contribute to maintaining the

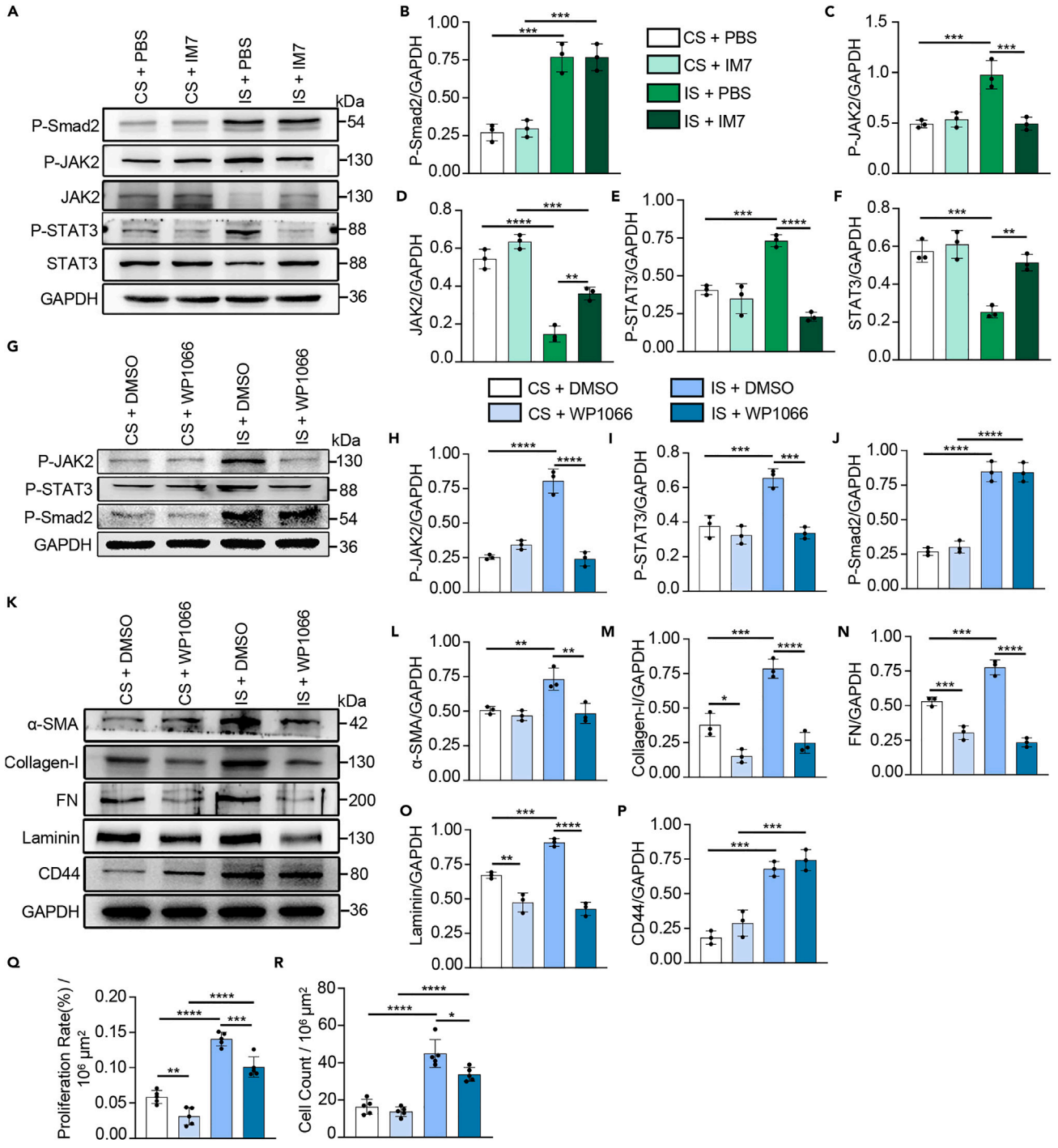

Figure 6. The JAK2/STAT3 signaling pathway participated in the CD44-mediated functional changes in fibroblasts

(A) Western blotting analyzed the expression of *p*-Smad2, *p*-JAK2, JAK2, p-STAT3, and STAT3 in the fibroblasts after IM7 treatment.

(B–F) Quantification of Western blotting results in A. N = 3 of each group by one-way ANOVA.

(G) Western blotting determined the expression of *p*-JAK2, p-STAT3, and *p*-Smad2 in the fibroblasts after WP1066 treatment.

(H–J) Quantification of western blotting results in G. N = 3 of each group by one-way ANOVA.

(K) Western blotting analyzed the expression of α-SMA, collagen-I, FN, laminin, and CD44 in the fibroblasts after WP1066 treatment.

(L–P) Quantification of western blotting results in K. N = 3 of each group by one-way ANOVA.

(Q and R) Quantification analysis of the rate of proliferation (%) (Q) per 10^6 μm^2 (n = 5) and cell numbers of migration (R) per 10^6 μm^2 (n = 5) in different groups by one-way ANOVA. All data were presented as mean ± SEM. (*p < 0.05, **p < 0.01, ***p < 0.001, ****p < 0.0001). (See also Figure S3).

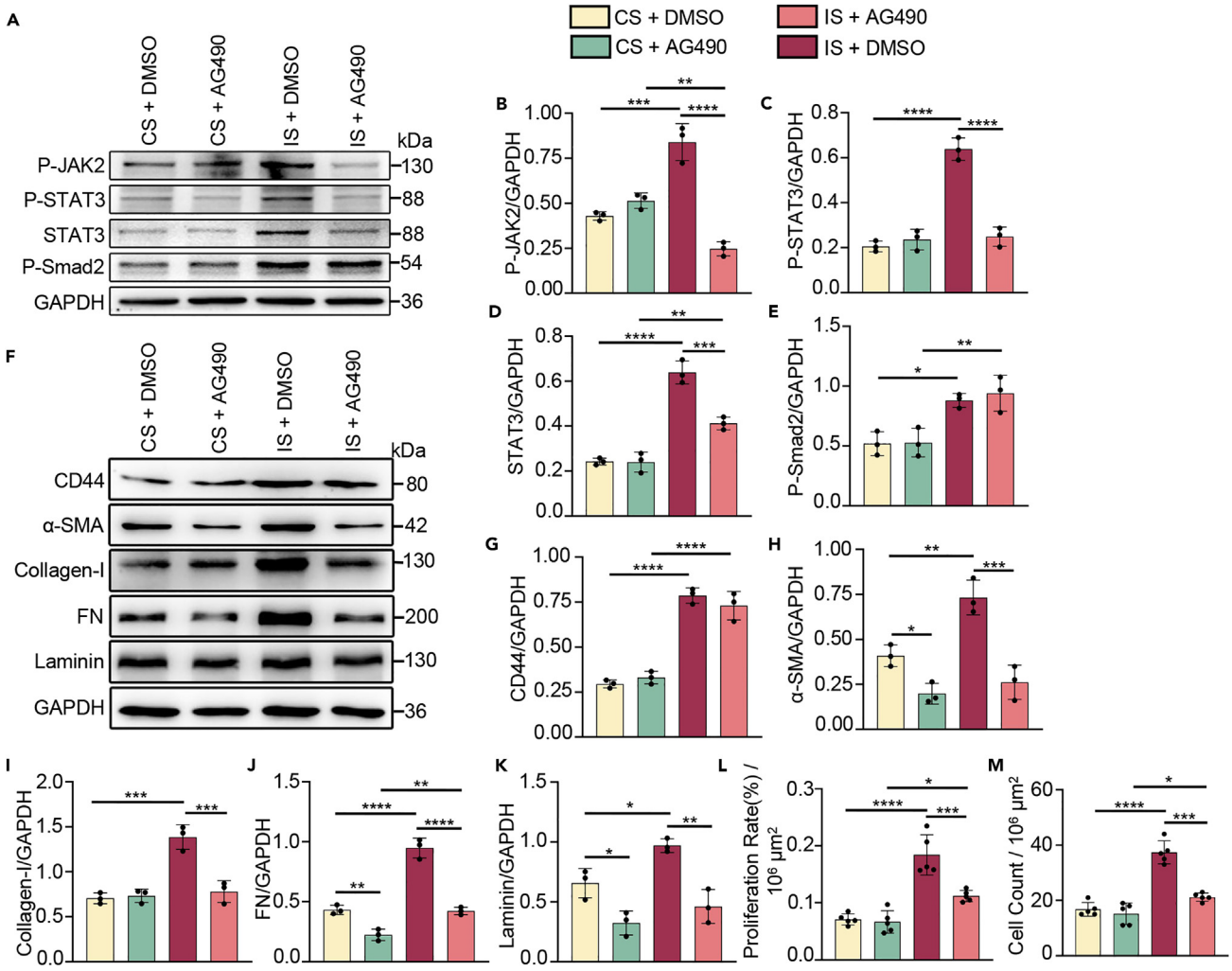

Figure 7. STAT3 was the downstream of JAK2 in CD44-mediated fibrotic effect in the inflammatory microenvironment

(A) Western blotting analyzed the expression of *p*-JAK2, p-STAT3, STAT3, and *p*-Smad2 in the fibroblasts stimulated with IS after inhibition of AG490.

(B–E) Quantification of western blotting results in A. N = 3 of each group by one-way ANOVA.

(F) Western blotting analyzed the expression of CD44, α-SMA, collagen-I, FN, and laminin in the fibroblasts stimulated with IS after inhibition of AG490.

(G–K) Quantification of western blotting results in F. N = 3 of each group by one-way ANOVA.

(L and M) Quantification analysis of the rate of proliferation (%) (L) per 10^6 μm^2 (n = 5) and cell numbers of migration (M) per 10^6 μm^2 (n = 5) in different groups by one-way ANOVA. All data were presented as mean ± SEM. (*p < 0.05, **p < 0.01, ***p < 0.001, ****p < 0.0001). (See also Figure S3).

stability of the three layers of the spinal cord meninges.[36] However, after SCI, fibroblasts are recruited to the injury site by inflammation factors. These activated fibroblasts undergo proliferation and secrete a large amount of ECMs, resulting in the formation of dense fibrotic scar tissue that hampers functional recovery of the spinal cord. Consequently, fibroblasts are considered to be potential targets for the treatment of fibrotic scar after SCI. However, several limitations need to be considered. Firstly, there is no specific fibroblast marker, which makes it difficult to selectively target fibroblasts to inhibit fibrotic scar formation.[3] Moreover, completely inhibiting fibrotic scar formation may not yield the most beneficial results, because the early presence of fibrotic scar tissue post-SCI prevents inflammation from spreading to surrounding tissues.[9] Therefore, targeting fibroblasts may not be the most optimal approach for addressing the challenge of fibrotic scar formation.

The inflammation response also plays a key role in the formation of fibrotic scar after SCI, presenting a potential therapeutic strategy. Numerous studies have demonstrated the effectiveness of anti-inflammatory treatments in reducing fibrotic scar.[37–44] However, clinical application is still in progress. For example, the use of methylprednisolone has been limited in recent years due to serious complications such as gastrointestinal bleeding and traumatic infection.[45] Moreover, inflammation in the early stage of injury can be beneficial to tissue repair.[10,11] Therefore, completely suppressing the inflammatory response after SCI may not be a sensible approach.

Given these considerations, our focus shifted to investigating the connection between inflammation and fibroblasts, as it may hold the key to achieving better outcomes.[37] In our study, we observed the upregulation of CD44, a key molecule involved in the inflammatory response and

fibrosis, after SCI *in vivo* and in the IS *in vitro*. Specifically, inhibiting the function of CD44 did not result in a complete decrease in the formation of the fibrotic scar. Furthermore, there was no significant difference in the expression of collagen-I, laminin, and α-SMA between the two dose groups when using the IM7 inhibitor 2 weeks after SCI, suggesting the blocking of fibrosis-related proteins by IM7 may not be dose-dependent. However, different effects were observed in GFAP expression. Western blotting results showed that high-dose IM7 (20 μg/day) treatment suppressed the expression of GFAP, whereas low-dose (10 μg/day) treatment did not. Additionally, compared to the PBS group, no significant reduction was observed after low-dose IM7 administration (Figures S2F and S2G), indicating that low-dose IM7 treatment mainly affected the formation of the fibrotic scar, but not the GFAP-related astrocyte scar. However, further experiments are required to address the underlying reasons for the difference between these two doses of IM7 treatment on astrocytes.

The TGF-β1/Smad signaling pathway is widely recognized for its involvement in fibrosis.[12] Thus, in order to investigate the molecular mechanism of CD44 in the formation of fibrotic scar after SCI, we initially examined whether CD44 could exert its function via the Smad pathway through phosphorylation of Smad2. However, IM7 did not alter the level of *p*-Smad2 under normal or inflammatory conditions (Figures 6A and 6B), which is consistent with findings from previous studies,[46] prompting us to explore alternative pathways. Previous research has demonstrated that IL-6 interacted with CD44 to activate STAT3 after lung injury and induced pulmonary fibrosis,[25] and this signal transduction might activate STAT3 by JAKs.[47] Thus, we hypothesized that JAK2/STAT3 might be a downstream molecule of CD44 involved in the inflammatory microenvironment. Our results demonstrated that blocking of CD44 inhibited JAK2/STAT3 activation. The functional changes observed in fibroblasts were effectively suppressed by the inhibition of JAK2/STAT3 signaling using WP1066. Interestingly, this inhibition did not have any impact on the expression of CD44 (Figures 6K and 6P). Consistently, when JAK2 was inhibited using AG490, similar results were observed, affecting the expression of p-STAT3. These findings strongly suggest that JAK2 plays a pivotal role in mediating the relationship between CD44 and STAT3.

Intriguingly, we observed that under AG490 treatment (50 μM), the expression of *p*-JAK2 in the CS was higher compared with that in the IS. This suggests a potential connection between AG490, the inflammatory environment, and a possible dose-dependent pattern. Prior studies have demonstrated that acute administration of AG490 *in vivo* dose-dependently alleviates thermal hyperalgesia.[48] To investigate whether a similar effect occurred in this study, we applied varying doses of AG490 (5 μM, 20 μM, and 50 μM) to BJ-1 cells in different environments (CS or IS), followed by western blotting analysis to evaluate *p*-JAK2 expression. The results indeed demonstrated a dose-dependent effect. Higher levels of *p*-JAK2 were observed in the inflammatory environment under low doses of AG490 (5 μM and 20 μM) treatment, while the high dose AG490 (50 μM) did not yield the same effect (Figures S3E and S3F). Subsequently, to determine whether ECM proteins could vary between high and low concentrations, we examined the expression of collagen-I in different groups under 20 μM AG490 treatment, and the results were consistent with those observed under 50 μM AG490 treatment (Figures S3G and S3H). Further studies are warranted to elucidate the intricate relationship between inflammation and AG490.

Based on these results, we postulated that in the inflammatory microenvironment, multiple types of cytokines and inflammatory factors secreted by activated macrophages can bind and activate CD44 on fibroblasts. Subsequently, the signal is transferred to the cytoplasm where it activates JAK2 and STAT3. The activated STAT3 enters into the cell nucleus and promotes fibrosis-related genes expression. Eventually, numerous fibroblasts proliferate, differentiate and migrate, accompanied by massive ECMs deposition. This leads to the formation of fibrotic scar (Figure 8).

Limitations of the study

However, it should be noted that JAK2/STAT3 signaling may not be the sole pathway implicated in CD44-mediated fibrosis. Our findings indicated that certain fibrosis-related proteins did not return to the control level in the presence of an inflammatory microenvironment, despite the inhibition of this pathway. This suggests the existence of other concurrent molecular pathways that may be involved in this process, or potentially non-CD44-dependent pathways like the Smad signaling pathways. Further investigations are warranted to substantiate these possibilities.

Conclusions

In conclusion, our findings suggest that a moderate inhibition of fibrotic scar formation could serve as a promising therapeutic strategy for its treatment. The results demonstrated that inhibition of CD44 and JAK2/STAT3 partly suppressed the formation of fibrotic scar and promoted functional recovery after SCI, which may be an effective therapeutic choice to alleviate fibrotic scar after SCI.

STAR★METHODS

Detailed methods are provided in the online version of this paper and include the following:

- KEY RESOURCES TABLE
- RESOURCE AVAILABILITY
  - Lead contact
  - Materials availability
  - Data and code availability
- EXPERIMENTAL MODEL AND SUBJECT DETAILS
  - Ethics statement

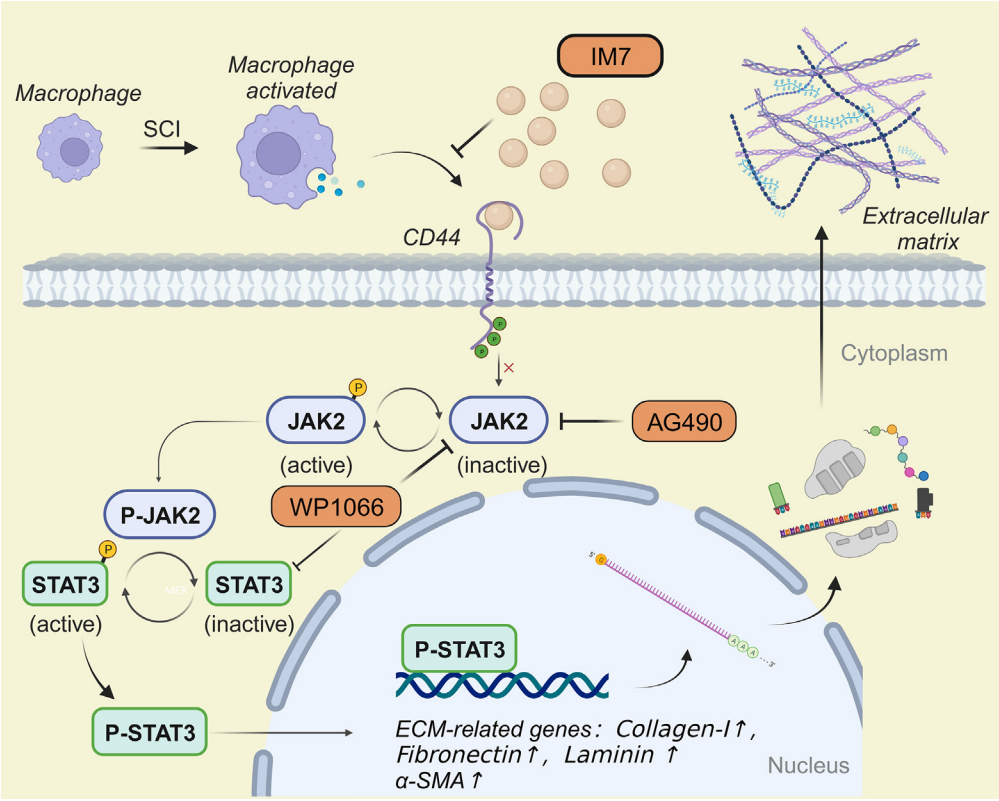

Figure 8. Diagram of molecule mechanism of CD44-JAK2-STAT3 in the fibroblasts following SCI, macrophages are activated and secrete varieties of cytokines and inflammatory factors, and recruit fibroblasts to participate in the subsequent repair process

Then CD44 on the fibroblasts would be activated by these proinflammatory factors, which could be inhibited by IM7. The signal is transferred into cells, and activates the JAK2 and STAT3. Activated STAT3 enters into nucleus and regulates the expression of fibrosis-related genes at the transcriptional level by binding specific DNA promoter sequences, which ultimately promotes the proliferation, differentiation, and migration of fibroblasts, leading to the deposition of excessive ECM proteins and finally forms dense fibrotic scar tissue.

SUPPLEMENTAL INFORMATION

Supplemental information can be found online at https://doi.org/10.1016/j.isci.2024.108935.

ACKNOWLEDGMENTS

We would like to thank all our colleagues in the Shusen Cui's Key Laboratory of Peripheral Nerve Injury and Regeneration for many insightful discussions and assistance.

Funding: This research was funded by National Natural Science Foundation of China (82271414), Jilin Province Scientific and Technological Development Program (YDZJ202301ZYTS017, 20190201059JC), Special Project on Health Talents of Jilin Province (2021SCZ01, 2021SCZ39, 2022SCZ24), Jilin Industrial Technology Research and Development Project (2023C040-4), Jilin Province Science and technology innovation platform construction project (YDZJ202302CXJD060), Spring Bud Program of China-Japan Union Hospital of Jilin University (2023CL05) and Bethune project of Jilin University (2023B19).

AUTHOR CONTRIBUTIONS

J.G. designed the research studies, conducted the experiments, acquired the data, analyzed the data, and wrote the manuscript. T.Y., X.X., K.M.Y., and L.L.S. performed the experiments and acquired the data. J.G., T.Y., and W.Z.Z. conducted the experiments. W.Z.L. provided reagents. R.J.C. provided the guidance on this study, analyzed data, and revised the manuscript. S.S.C. and X.S.G. supervised the study, provided the reagents and guidance on this study.

DECLARATION OF INTERESTS

The authors declare no competing interests.

Received: August 8, 2023
Revised: November 17, 2023
Accepted: January 12, 2024
Published: January 16, 2024

REFERENCES

1. Lee, B.B., Cripps, R.A., Fitzharris, M., and Wing, P.C. (2014). The global map for traumatic spinal cord injury epidemiology: update 2011, global incidence rate. Spinal Cord *52*, 110–116.
2. Brazda, N., and Müller, H.W. (2009). Pharmacological modification of the extracellular matrix to promote regeneration of the injured brain and spinal cord. Prog. Brain Res. *175*, 269–281.
3. Soderblom, C., Luo, X., Blumenthal, E., Bray, E., Lyapichev, K., Ramos, J., Krishnan, V., Lai-Hsu, C., Park, K.K., Tsoulfas, P., and Lee, J.K. (2013). Perivascular fibroblasts form the fibrotic scar after contusive spinal cord injury. J. Neurosci. *33*, 13882–13887.
4. Dorrier, C.E., Jones, H.E., Pintarić, L., Siegenthaler, J.A., and Daneman, R. (2022). Emerging roles for CNS fibroblasts in health, injury and disease. Nat. Rev. Neurosci. *23*, 23–34.
5. Dani, N., Herbst, R.H., McCabe, C., Green, G.S., Kaiser, K., Head, J.P., Cui, J., Shipley, F.B., Jang, A., Dionne, D., et al. (2021). A cellular and spatial map of the choroid plexus across brain ventricles and ages. Cell *184*, 3056–3074.e21.
6. Vanlandewijck, M., He, L., Mäe, M.A., Andrae, J., Ando, K., Del Gaudio, F., Nahar, K., Lebouvier, T., Laviña, B., Gouveia, L., et al. (2018). A molecular atlas of cell types and zonation in the brain vasculature. Nature *554*, 475–480.
7. Zhu, Y., Soderblom, C., Trojanowsky, M., Lee, D.H., and Lee, J.K. (2015). Fibronectin Matrix Assembly after Spinal Cord Injury. J. Neurotrauma *32*, 1158–1167.
8. O'Shea, T.M., Burda, J.E., and Sofroniew, M.V. (2017). Cell biology of spinal cord injury and repair. J. Clin. Invest. *127*, 3259–3270.
9. Dorrier, C.E., Aran, D., Haenelt, E.A., Sheehy, R.N., Hoi, K.K., Pintarić, L., Chen, Y., Lizama, C.O., Cautivo, K.M., Weiner, G.A., et al. (2021). CNS fibroblasts form a fibrotic scar in response to immune cell infiltration. Nat. Neurosci. *24*, 234–244.
10. Schäfer, M.K.E., and Tegeder, I. (2018). NG2/CSPG4 and progranulin in the posttraumatic glial scar. Matrix Biol. *68–69*, 571–588.
11. Zhu, Y., Soderblom, C., Krishnan, V., Ashbaugh, J., Bethea, J.R., and Lee, J.K. (2015). Hematogenous macrophage depletion reduces the fibrotic scar and increases axonal growth after spinal cord injury. Neurobiol. Dis. *74*, 114–125.
12. Tran, A.P., Warren, P.M., and Silver, J. (2018). The Biology of Regeneration Failure and Success After Spinal Cord Injury. Physiol. Rev. *98*, 881–917.
13. Wang, W., Liu, R., Su, Y., Li, H., Xie, W., and Ning, B. (2018). MicroRNA-21-5p mediates TGF-β-regulated fibrogenic activation of spinal fibroblasts and the formation of fibrotic scars after spinal cord injury. Int. J. Biol. Sci. *14*, 178–188.
14. Rice, L.M., Padilla, C.M., McLaughlin, S.R., Mathes, A., Ziemek, J., Goummih, S., Nakerakanti, S., York, M., Farina, G., Whitfield, M.L., et al. (2015). Fresolimumab treatment decreases biomarkers and improves clinical symptoms in systemic sclerosis patients. J. Clin. Invest. *125*, 2795–2807.
15. Petukhov, D., Richter-Dayan, M., Fridlender, Z., Breuer, R., and Wallach-Dayan, S.B. (2019). Increased Regeneration Following Stress-Induced Lung Injury in Bleomycin-Treated Chimeric Mice with CD44 Knockout Mesenchymal Cells. Cells *8*, 1211.
16. Li, S., Li, C., Zhang, Y., He, X., Chen, X., Zeng, X., Liu, F., Chen, Y., and Chen, J. (2019). Targeting Mechanics-Induced Fibroblast Activation through CD44-RhoA-YAP Pathway Ameliorates Crystalline Silica-Induced Silicosis. Theranostics *9*, 4993–5008.
17. Teder, P., Vandivier, R.W., Jiang, D., Liang, J., Cohn, L., Puré, E., Henson, P.M., and Noble, P.W. (2002). Resolution of lung inflammation by CD44. Science *296*, 155–158.
18. Suleiman, M., Abdulrahman, N., Yalcin, H., and Mraiche, F. (2018). The role of CD44, hyaluronan and NHE1 in cardiac remodeling. Life Sci. *209*, 197–201.
19. Ponta, H., Sherman, L., and Herrlich, P.A. (2003). CD44: from adhesion molecules to signalling regulators. Nat. Rev. Mol. Cell Biol. *4*, 33–45.
20. Jordan, A.R., Racine, R.R., Hennig, M.J.P., and Lokeshwar, V.B. (2015). The Role of CD44 in Disease Pathophysiology and Targeted Treatment. Front. Immunol. *6*, 182.
21. Basakran, N.S. (2015). CD44 as a potential diagnostic tumor marker. Saudi Med. J. *36*, 273–279.
22. Senbanjo, L.T., and Chellaiah, M.A. (2017). CD44: A Multifunctional Cell Surface Adhesion Receptor Is a Regulator of Progression and Metastasis of Cancer Cells. Front. Cell Dev. Biol. *5*, 18.
23. Puré, E., and Cuff, C.A. (2001). A crucial role for CD44 in inflammation. Trends Mol. Med. *7*, 213–221.
24. Cuff, C.A., Kothapalli, D., Azonobi, I., Chun, S., Zhang, Y., Belkin, R., Yeh, C., Secreto, A., Assoian, R.K., Rader, D.J., and Puré, E. (2001). The adhesion receptor CD44 promotes atherosclerosis by mediating inflammatory cell recruitment and vascular cell activation. J. Clin. Invest. *108*, 1031–1040.
25. Kasembeli, M.M., Bharadwaj, U., Robinson, P., and Tweardy, D.J. (2018). Contribution of STAT3 to Inflammatory and Fibrotic Diseases and Prospects for its Targeting for Treatment. Int. J. Mol. Sci. *19*, 2299.
26. Pulivendala, G., Bale, S., and Godugu, C. (2020). Honokiol: A polyphenol neolignan ameliorates pulmonary fibrosis by inhibiting TGF-β/Smad signaling, matrix proteins and IL-6/CD44/STAT3 axis both in vitro and in vivo. Toxicol. Appl. Pharmacol. *391*, 114913.
27. Zhang, Y., Dees, C., Beyer, C., Lin, N.Y., Distler, A., Zerr, P., Palumbo, K., Susok, L., Kreuter, A., Distler, O., et al. (2015). Inhibition of casein kinase II reduces TGFβ induced fibroblast activation and ameliorates experimental fibrosis. Ann. Rheum. Dis. *74*, 936–943.
28. Wanner, I.B., Anderson, M.A., Song, B., Levine, J., Fernandez, A., Gray-Thompson, Z., Ao, Y., and Sofroniew, M.V. (2013). Glial scar

borders are formed by newly proliferated, elongated astrocytes that interact to corral inflammatory and fibrotic cells via STAT3-dependent mechanisms after spinal cord injury. J. Neurosci. *33*, 12870–12886.
29. Tran, A.P., Warren, P.M., and Silver, J. (2022). New insights into glial scar formation after spinal cord injury. Cell Tissue Res. *387*, 319–336.
30. Anderson, M.A., Burda, J.E., Ren, Y., Ao, Y., O'Shea, T.M., Kawaguchi, R., Coppola, G., Khakh, B.S., Deming, T.J., and Sofroniew, M.V. (2016). Astrocyte scar formation aids central nervous system axon regeneration. Nature *532*, 195–200.
31. Wahane, S., and Sofroniew, M.V. (2022). Loss-of-function manipulations to identify roles of diverse glia and stromal cells during CNS scar formation. Cell Tissue Res. *387*, 337–350.
32. Hawkins, L.A., and Devitt, A. (2013). Current understanding of the mechanisms for clearance of apoptotic cells-a fine balance. J. Cell Death *6*, 57–68.
33. Fan, B., Wei, Z., Yao, X., Shi, G., Cheng, X., Zhou, X., Zhou, H., Ning, G., Kong, X., and Feng, S. (2018). Microenvironment Imbalance of Spinal Cord Injury. Cell Transplant. *27*, 853–866.
34. Orr, M.B., and Gensel, J.C. (2018). Spinal Cord Injury Scarring and Inflammation: Therapies Targeting Glial and Inflammatory Responses. Neurotherapeutics *15*, 541–553.
35. D'Ambrosi, N., and Apolloni, S. (2020). Fibrotic Scar in Neurodegenerative Diseases. Front. Immunol. *11*, 1394.
36. Mastorakos, P., and McGavern, D. (2019). The anatomy and immunology of vasculature in the central nervous system. Sci. Immunol. *4*, eaav0492.
37. Gensel, J.C., Kopper, T.J., Zhang, B., Orr, M.B., and Bailey, W.M. (2017). Predictive screening of M1 and M2 macrophages reveals the immunomodulatory effectiveness of post spinal cord injury azithromycin treatment. Sci. Rep. *7*, 40144.
38. Francos-Quijorna, I., Amo-Aparicio, J., Martinez-Muriana, A., and López-Vales, R. (2016). IL-4 drives microglia and macrophages toward a phenotype conducive for tissue repair and functional recovery after spinal cord injury. Glia *64*, 2079–2092.
39. Lima, R., Monteiro, S., Lopes, J.P., Barradas, P., Vasconcelos, N.L., Gomes, E.D., Assunção-Silva, R.C., Teixeira, F.G., Morais, M., Sousa, N., et al. (2017). Systemic Interleukin-4 Administration after Spinal Cord Injury Modulates Inflammation and Promotes Neuroprotection. Pharmaceuticals *10*, 83.
40. Coll-Miró, M., Francos-Quijorna, I., Santos-Nogueira, E., Torres-Espin, A., Bufler, P., Dinarello, C.A., and López-Vales, R. (2016). Beneficial effects of IL-37 after spinal cord injury in mice. Proc. Natl. Acad. Sci. USA *113*, 1411–1416.
41. Dooley, D., Lemmens, E., Vangansewinkel, T., Le Blon, D., Hoornaert, C., Ponsaerts, P., and Hendrix, S. (2016). Cell-Based Delivery of Interleukin-13 Directs Alternative Activation of Macrophages Resulting in Improved Functional Outcome after Spinal Cord Injury. Stem Cell Rep. *7*, 1099–1115.
42. Li, Y., Ritzel, R.M., Khan, N., Cao, T., He, J., Lei, Z., Matyas, J.J., Sabirzhanov, B., Liu, S., Li, H., et al. (2020). Delayed microglial depletion after spinal cord injury reduces chronic inflammation and neurodegeneration in the brain and improves neurological recovery in male mice. Theranostics *10*, 11376–11403.
43. Shen, K., Sun, G., Chan, L., He, L., Li, X., Yang, S., Wang, B., Zhang, H., Huang, J., Chang, M., et al. (2021). Anti-Inflammatory Nanotherapeutics by Targeting Matrix Metalloproteinases for Immunotherapy of Spinal Cord Injury. Small *17*, e2102102.
44. Zeng, H., Liu, N., Yang, Y.Y., Xing, H.Y., Liu, X.X., Li, F., La, G.Y., Huang, M.J., and Zhou, M.W. (2019). Lentivirus-mediated downregulation of α-synuclein reduces neuroinflammation and promotes functional recovery in rats with spinal cord injury. J. Neuroinflammation *16*, 283.
45. Liu, Z., Yang, Y., He, L., Pang, M., Luo, C., Liu, B., and Rong, L. (2019). High-dose methylprednisolone for acute traumatic spinal cord injury: A meta-analysis. Neurology *93*, e841–e850.
46. Wang, Y., Mack, J.A., and Maytin, E.V. (2019). CD44 inhibits α-SMA gene expression via a novel G-actin/MRTF-mediated pathway that intersects with TGFβR/p38MAPK signaling in murine skin fibroblasts. J. Biol. Chem. *294*, 12779–12794.
47. Bharadwaj, U., Kasembeli, M.M., Robinson, P., and Tweardy, D.J. (2020). Targeting Janus Kinases and Signal Transducer and Activator of Transcription 3 to Treat Inflammation, Fibrosis, and Cancer: Rationale, Progress, and Caution. Pharmacol. Rev. *72*, 486–526.
48. Cheppudira, B.P., Garza, T.H., Petz, L.N., Clifford, J.L., and Fowler, M. (2015). Anti-hyperalgesic effects of AG490, a Janus kinase inhibitor, in a rat model of inflammatory pain. Biomed. Rep. *3*, 703–706.
49. Liu, K., Lu, Y., Lee, J.K., Samara, R., Willenberg, R., Sears-Kraxberger, I., Tedeschi, A., Park, K.K., Jin, D., Cai, B., et al. (2010). PTEN deletion enhances the regenerative ability of adult corticospinal neurons. Nat. Neurosci. *13*, 1075–1081.
50. Basso, D.M., Fisher, L.C., Anderson, A.J., Jakeman, L.B., McTigue, D.M., and Popovich, P.G. (2006). Basso Mouse Scale for locomotion detects differences in recovery after spinal cord injury in five common mouse strains. J. Neurotrauma *23*, 635–659.
51. Li, Z., Yu, S., Liu, Y., Hu, X., Li, Y., Xiao, Z., Chen, Y., Tian, D., Xu, X., Cheng, L., et al. (2022). SU16f inhibits fibrotic scar formation and facilitates axon regeneration and locomotor function recovery after spinal cord injury by blocking the PDGFRβ pathway. J. Neuroinflammation *19*, 95.
52. Dias, D.O., Kalkitsas, J., Kelahmetoglu, Y., Estrada, C.P., Tatarishvili, J., Holl, D., Jansson, L., Banitalebi, S., Amiry-Moghaddam, M., Ernst, A., et al. (2021). Pericyte-derived fibrotic scarring is conserved across diverse central nervous system lesions. Nat. Commun. *12*, 5501.

STAR★METHODS

KEY RESOURCES TABLE

REAGENT or RESOURCE	SOURCE	IDENTIFIER
Antibodies		
Mouse monoclonal anti-CD44	Cell Signaling Technology	Cat# 5640; RRID: AB_10547133
Mouse monoclonal anti-CD44	Abmart	Cat#MB9213; RRID: AB_3083700
Rabbit monoclonal anti-CD44	Abmart	Cat#TD6392; RRID: AB_3083701
Rabbit monoclonal anti-Thy-1	Abmart	Cat#T55335; RRID: AB_3083702
Rabbit monoclonal anti-Collagen-I	Abcam	Cat# ab34710; RRID: AB_731684
Rabbit monoclonal anti-Collagen-I	Abmart	Cat#TA7001; RRID: AB_2936833
Rabbit monoclonal anti-alpha smooth muscle Actin	Abmart	Cat#T55295; RRID: AB_2892572
Rabbit monoclonal anti-Laminin	Abcam	Cat# ab11575; RRID: AB_298179
Rabbit monoclonal anti-Fibronectin	Abcam	Cat# ab6328; RRID: AB_305428
Mouse monoclonal anti-GFAP	Millipore	Cat# MAB360; RRID: AB_11212597
Mouse monoclonal anti-*p*-Smad2/3	Santa Cruz Biotechnology	Cat# sc-517575; RRID: AB_2892229
Rabbit monoclonal anti-JAK2	Abmart	Cat#T55287; RRID: AB_3076704
Rabbit monoclonal anti-*p*-JAK2	Abmart	Cat#T56570; RRID: AB_2936394
Rabbit monoclonal anti-STAT3	Abmart	Cat#T55292; RRID: AB_3083703
Rabbit monoclonal anti-p-STAT3	Abmart	Cat#T56566; RRID: AB_2936393
Donkey anti-Rabbit IgG (H + L) Highly Cross-Adsorbed Secondary Antibody, Alexa Fluor™ 546	Invitrogen	Cat# A10040; RRID: AB_2534016
Goat anti-Mouse IgG (H + L) Highly Cross-Adsorbed Secondary Antibody, Alexa Fluor™ 546	Invitrogen	Cat# A11030; RRID: AB_2534089
Donkey anti-Mouse IgG (H + L) Highly Cross-Adsorbed Secondary Antibody, Alexa Fluor™ 488	Invitrogen	Cat# A21202; RRID: AB_141607
Goat anti-Rabbit IgG (H + L) Cross-Adsorbed Secondary Antibody, Alexa Fluor™ 488	Invitrogen	Cat# A-11008; RRID: AB_143165
Streptavidin Alexa 647	Jackson Immunoresearch Laboratories	Cat#016-600-084; RRID: AB_2341101
HRP-labeled Goat Anti-Rabbit IgG(H + L)	Beyotime	Cat#A0208; RRID: AB_2892644
HRP-labeled Goat Anti-Mouse IgG(H + L)	Beyotime	Cat#A0216; RRID: AB_2860575
ProteinFind® Anti-GAPDH Mouse Monoclonal Antibody	TransGen	Cat#HC301-02; RRID: AB_2629434
ProteinFind® Anti-β-Tubulin Mouse Monoclonal Antibody	TransGen	Cat#HC101-02; RRID: AB_2893358
Biological samples		
C57 BL/6 mice	Liaoning Changsheng biotechbology co.,Ltd	https://www.lncssw.com/
Chemicals, peptides, and recombinant proteins		
In Vivo Mab anti-mouse/human CD44 (IM7)	Bio X cell	751121M2, Cat#BE0039;RRID:AB_1107649
WP1066	Targetmol	Cat#T2156;CAS:857064-38-1;Batch:144277
AG490	Targetmol	Cat#T2600;CAS:133550-30-8;Batch:147766
PageRuler Prestained Protein Ladder (10–180 kDa)	Thermo Fisher	Cat#26616
PageRuler Plus Prestained Protein Ladder (10–250 kDa)	Thermo Fisher	Cat#26619
PageRuler Plus Prestained Protein Ladder (6.5–270 kDa)	Bio-platform	Cat#BP117

(*Continued on next page*)

Continued

REAGENT or RESOURCE	SOURCE	IDENTIFIER
Biotinylated dextran amine 10000	Invitrogen	Cat#D1956
Lipopolysaccharide	Sigma	Cat#L4391
RIPA lysis buffer	Sangon Biotech, Shanghai, China	Cat#500008
bicinchoninic acid assay	Beyotime Biotechnology	#P0010
Critical commercial assays		
Cell-Light EdU Apollo567	Guangzhou RiboBio	C10310-1
Cell Transwell Kit	CORNING, Shanghai, China	3422
Kdl U40 insulin needle	Shanghai Kindly Medical Instruments Co.,Ltd	https://www.kdl-int.com/
Experimental models: Cell lines		
Mouse: Raw 264.7	ATCC	TIB-71
Human: BJ-1	ATCC	CRL-2522
Experimental models: Organisms/strains		
C57 BL/6 mice	Liaoning Changsheng biotechbology co.,Ltd	https://www.lncssw.com/
Software and algorithms		
SPSS	v. 21.0; SPSS, Inc., Chicago, IL, USA	https://spss.en.softonic.com/
GraphPad Prism	La Jolla, CA	https://www.graphpad.com/
ImageJ	1.47v	https://fiji.sc/
BioRender	49 Spadina Ave. Suite 200 Toronto ON M5V 2J1 Canada	www.biorender.com

RESOURCE AVAILABILITY

Lead contact

Further information and requests for resources and reagents should be directed to and will be fulfilled by the lead contact, R Cao (caorj@jlu.edu.cn) or S Cui (cuiss@jlu.edu.cn).

Materials availability

This study did not generate new unique reagents.

Data and code availability

All data reported in this paper will be shared by the lead contact upon request. This paper does not report original code. Any additional information required to reanalyze the data reported in this paper is available from the lead contact upon request.

EXPERIMENTAL MODEL AND SUBJECT DETAILS

Ethics statement

Animal research using mice was conducted in accordance with the US National Institute of Health (NIH) Guide for the Care and Use of Laboratory Animals and were approved by the Jilin University Administration Committee of Experimental Animals.

Animals

All mice were healthy, immune competent and drug and test naive. C57 BL/6 female mice aged 8–10 weeks weighing 20–22 g were used. The mice were provided with a normal diet and had *ad libitum* access to water at room temperature (25°C) with a 12 h light/dark cycle. All mice were randomly assigned to experimental groups.

Cell lines

Raw 264.7 (mouse [*Mus musculus*] ascites macrophages) and BJ-1 cell lines (human [*Homo sapiens*] skin fibroblast) were all obtained and authenticated from ATCC (https://www.atcc.org/). These two cell lines were cultured in Dulbecco's Modified Eagle Medium (DMEM, high-glucose, Gibco, USA) supplemented with 10% FBS (Sigma, USA) and 1% Penicillin-Streptomycin Solution (PS, 100 ×, Beyotime, China). All cell lines were incubated at 37°C with 5% CO_2.

METHOD DETAILS

Spinal cord crush injury model

Female mice were completely anesthetized (isoflurane, 2.5% for induction and 2% for maintenance) and placed in a prone position on the operating table. After sterilization, a longitudinal incision of approximately 2 cm was made in the direction of the spinal spinous process around T10.The spinous process and conical plate were removed to expose the entire spinal cord. A No.5 Dumont forceps was then inserted perpendicular to the longitudinal axis of the T10 spinal cord, ensuring that the tips of the forceps were located on both sides of the spinal cord and reached the ventral wall of the spinal canal. The forceps were clamped completely and held for 5 s. Immediately after clamping, a horizontal line of blood-filled marks appeared at the clamping site, indicating the successful construction of the model. Finally, the incision was sutured layer by layer. Postoperative anti-infection treatment (Baytril antibiotic, 2.5 mg/kg in 1 mL sterile saline, subcutaneously) was administered for 3 days, and routine urine care was provided twice a day after surgery.

Intrathecal injection of IM7

IM7 (BioXCell, BE0039) was diluted to concentrations of 1 μg/μL and 0.5 μg/μL using sterile PBS. The mice were anesthetized in a prone position on the operating table. The bilateral iliac bones were fixed, and the L5-L6 intervertebral space was determined as the injection location. The apparent sudden tail swing was an indicator of successful intervertebral insertion. Then, 20 μL of IM7 diluent was injected using a U40 insulin needle (kdl, 0.3 × 8 mm) at a rate of 1 μL/4 s. The needle position was maintained for approximately 3 min after injection, and then the syringe was gently rotated and withdrawn to avoid leakage.

BDA cerebral cortex injection

BDA (Biotinylated dextran amine 10000, Invitrogen D1956) was used to label the corticospinal tract (CST). After anesthesia, the mice were fixed in a prone position on the operating table. BDA (10% w/v) was injected into the left cerebral cortex at 4 sites (AP coordinates from bregma in mm: AP 1.0/1.5, 0.5/1.5, −0.5/1.5, −1.0/1.5 all at a depth of 0.5 mm into cortex).[49] Each site received an injection of 0.5 μL (total 2 μL) at a rate of 0.1 μL/min. After the injection, the needle was left in place for 3 min, and then slowly withdrawn to prevent leakage. The scalp and skin were sutured, and postoperative care was provided.

Immunohistochemical staining

Spinal cord samples (two spinal cord segments of T8-T12 in each sample) were fixed overnight in a 4% PFA solution. The tissues were then routinely processed by dehydration and embedding before the frozen tissue sections of 10–12 mm thickness (25mm thickness for BDA staining) were prepared for staining. After washing with PBS at least three times, the sections were blocked with a solution of 5% BSA (Genview, USA) +1% Triton X-100 (Genview, USA) for 1 h at room temperature. Following the incubation overnight at 4°C with primary antibodies (anti-CD44 (1:200, Abmart), anti-Thy-1 (1:100, Abmart), anti-collagen-I (1:100, Abcam), anti-fibronectin (1:100, Abcam), anti-laminin (1:100, Abcam), anti-α-SMA (1:100, Abmart) and anti-GFAP (1:500, Abcam)), the sections were subsequently incubated with a secondary antibody (Alexa Fluor 546 and Alexa Fluor 488, 1:500, Invitrogen, CA, USA. Streptavidin Alexa 647,1:500, Jackson Immunoresearch Laboratories) for 2 h at room temperature. Finally, the sections were washed three times and analyzed using a Laser Confocal Electron Microscope (Nikon, Japan).

Protein isolation and western blotting

Fibroblasts and spinal cord tissues (two spinal cord segments of T8-T12 in each sample) were prepared using RIPA lysis buffer (#C500008; Sangon Biotech, Shanghai, China). The protein concentrations were determined using the bicinchoninic acid assay (#P0010, Beyotime Biotechnology). Protein samples were separated by 10% SDS-PAGE and transferred onto PVDF membranes. The membranes were then blocked with 5% BSA in tris-buffered saline with Tween 20 for 2 h at room temperature and incubated overnight at 4°C with primary antibodies (anti-CD44 (1:1000, Abmart), anti-collagen-I (1:2000, Abcam), anti-fibronectin (1:1000, Abcam), anti-laminin (1:1000, Abcam), anti-α-SMA (1:5000, Abmart) and anti-GFAP (1:2000, Abcam), anti-*p*-Smad2 (1:1000, Abmart), anti-*p*-JAK2 (1:1000, Abmart), anti-STAT3 (1:1000, Abmart) and anti-p-STAT3 (1:1000, Abmart)). Subsequently, the membranes were detected using an HRP-conjugated secondary antibody for 2 h at room temperature. Finally, the images were scanned using a GS800 Densitometer Scanner, and the blotting intensity was assessed using Multi Gauge software (Fuji, Tokyo, Japan). Western blotting was repeated three times for the statistical analysis. The intensity of target proteins was related to that of GAPDH or β-Tubulin.

Macrophage supernatant collection

Lipopolysaccharide (LPS, L4391, Sigma) and an equal amount of PBS were added to the Raw macrophage medium at a ratio of 1:1000. After 24h, the supernatants from both groups were collected, centrifuged (1000 r/min, 10 min), and filtered (0.22 μm). The collected supernatants were stored at −20°C.

Cell proliferation assay

BJ-1 fibroblasts were cultured in 96-well plates. IM7 (10 μg/mL) and an equal amount of PBS were added for pretreatment for 12 h. Subsequently, inflammatory supernatant (IS, 100 μL) and control supernatant (CS, 100 μL) were added respectively. The subsequent experiments

were performed according to the instructions of the EdU kit (Cell-Light EdU Apollo567, C10310-1, Guangzhou RiboBio). The cells were incubated for 2 h. Finally, the positive cells were observed and counted under a microscope. The mean proliferation rate per 10^6 μm^2 (mean proliferation rate = number of proliferating cells (red)/the number of total cells (blue) ×100%) was used to represent the ability of fibroblasts proliferation.

The same procedures were adopted in the experiments involving WP1066 (5 μmol/L, T2156, Targetmol) and AG490 (50 μmol/L, T2600, Targetmol), while the processing time of these two inhibitors was reset to 1 h and 24 h, respectively (control groups with equal volumes of DMSO).

Cell migration assay

BJ-1 fibroblasts were cultured in the upper layer of a Transwell Chamber (3422, CORNING, Shanghai, China). IM7 (10 μg/mL) or PBS were added for pretreatment of 12 h. Subsequently, inflammatory supernatant (IS, 100 μL) and control supernatant (CS, 100 μL) were added, respectively. After 24h, the medium was removed, and the transwell chamber was fixed with 4% PFA at room temperature for 10min. It was then washed 1–2 times with PBS, stained with 0.1% crystal violet for 8 min, and the staining solution was discarded. After washing 1–2 times, the upper layer of the chambers was gently wiped, and the positive cells were observed and counted under a microscope. Five images (10^6 μm^2) from each group were selected and independently assessed by unbiased observers to represent the migration ability of BJ-1 cells under different conditions. The same procedures were performed for the experiments involving WP1066 and AG490, with the processing time for these two inhibitors reset to 1 h and 24 h, respectively (control groups with equal volumes of DMSO).

Behavioral tests

The recovery of spinal cord function was recorded by observing the BMS score and conducting the tail-flick test. (1) BMS scores: Mice were assigned scores ranging from 0 to 9 based on the Basso Mouse Scale.[50] (2) Tail-flick test: Mice were gently held by hand with a terry glove. A thermostatic water bath was set at 52°C, and the exposed distal part of the tail (3 cm) was immersed into hot water. The tail-flick latency was defined as the time required for a mouse to flick or remove its tail out of hot water. A maximum cut-off value of 15 s was set to avoid thermal injury. Tail-flick latency was assessed before and after drug injection. Each mouse was recorded 4 times at intervals of 3–5 min.

Quantification for IHC

Quantification of immunohistochemical images was performed using the ImageJ 1.47v software in a blind fashion. The immunoreactivities of $GFAP^-$ (considered as the fibrotic scar), Collagen-I^+ and $GFAP^+$ were normalized to the area of the spinal cord segment spanning the injured core in a 10 × image. Immunoreactivities of these areas were determined by thresholding above background level and calculating the area covered by the thresholded regions using ImageJ. For each animal, sections including the injury epicenter and two adjacent sagittal sections spaced 200 μm apart were quantified. The counts from each section were then averaged, with three samples per group.[9,51]

To determine the lesion area, sections were immunostained for Collagen-I, GFAP, and DAPI. The lesions were defined as the GFAP negative area within the GFAP-defined borders filled with Collagen-I^+ areas. Area measurements were carried out using the ImageJ 1.47v software in a blind fashion. The areas of lesions were normalized to the area of the spinal cord segment spanning the injured core in a 10 × image. All quantifications were done at least three alternate sections per animal covering the lesion epicenter and spaced 200 μm apart. The counts from each section were then averaged, with three samples per group.[52]

QUANTIFICATION AND STATISTICAL ANALYSIS

All data in this study were expressed as mean ± SEM, and analyzed using SPSS software (v. 21.0; SPSS, Inc., Chicago, IL, USA) and GraphPad Prism Software 8.4.2 (La Jolla, CA). two-way ANOVA or one-way ANOVA were performed for the comparison among multiple groups, followed by post-hoc Tukey's test. Unpaired Student's *t* test was used for the comparison between two groups. All experiments were performed at least three times independently. *$p < 0.05$ was considered statistically significant, with additional levels of significance indicated as **$p < 0.01$, ***$p < 0.001$, ****$p < 0.0001$.